Electric double layer on fractal electrodes

Hidetsugu Sakaguchi and Reisei Baba
Department of Applied Science for Electronics and Materials, Interdisciplinary Graduate School of Engineering Sciences, Kyushu University, Kasuga, Fukuoka 816-8580, Japan

(Received 12 December 2006; revised manuscript received 2 February 2007; published 9 May 2007)

The electric double layer around fractal electrodes is studied with direct numerical simulations of the Nernst-Planck equation coupled with the Poisson equation. The capacitance and the relaxation time obey a power law as a function of the system size, the temperature, and the concentration. The time evolution of the charging process exhibits a stretched exponential law, and the exponent β is numerically evaluated.

DOI: 10.1103/PhysRevE.75.051502 PACS number(s): 82.45.−h, 05.45.Df, 66.10.Cb

I. INTRODUCTION AND MODEL EQUATION

The electric double layer plays an important role in various research fields such as plasma physics, electrochemistry, and colloidal science. Electric double-layer capacitors (EDLCs) are electric devices with large capacitance using the electric double layer [1,2]. Activated carbon is used as electrode materials in EDLCs. The high capacitance is caused by the large surface area in the random porous media. The rough surfaces in porous media are often characterized by the fractal dimension [3]. It is important to understand the electric double layer in fractal media. In this paper, we study the charging dynamics of the electric double layer on fractal electrodes. Because geometrical properties such as the fractal dimension are well-known, we use a diffusion-limited aggregation (DLA) cluster and a critical percolation cluster as a simple random fractal electrode in two dimensions, although they are not so realistic models for EDLCs. We study a simple dynamical model for the electric double layer around the fractal electrodes and do not consider many effects such as finite-length-dipole effects and steric effects of finite ion size, although they are important in realistic EDLCs [4,5].

The electric double layer on the fractal electrode has been often studied using electric circuit models [6,7]. In this paper, we study the electric double layer by the direct numerical simulation of a dynamical version of the Gouy-Chapman model in electrochemistry [8,9]. In the Gouy-Chapman model, the electric double layer is constructed only with the diffusion double layer. That is, we do not consider the Helmholtz layer for the sake of simplicity. The electric potential obeys the Poisson equation. Positive and negative ions satisfy the Nernst-Planck equations. The coupled model equations are written as

$$\frac{\partial \rho_+}{\partial t} = D_+ \nabla^2 \rho_+ + \mu_+ e \nabla (\rho_+ \nabla \phi),$$

$$\frac{\partial \rho_-}{\partial t} = D_- \nabla^2 \rho_- - \mu_- e \nabla (\rho_- \nabla \phi),$$

$$\nabla^2 \phi = \frac{e}{\epsilon}(\rho_- - \rho_+), \tag{1}$$

where ϕ is the electric potential, ρ_+ and ρ_- denote the concentration of the positive and negative ions, $D_\pm$ denotes the diffusion constant for ions, $\mu_\pm$ is the mobility of ions, and ϵ is the dielectric constant. We assume further that the charge of each ion is $\pm e$, and the mobility of each ion is the same $\mu_+ = \mu_- = \mu$ for the sake of simplicity. Owing to the Einstein relation, the diffusion constant and the mobility satisfy the relation $D_+ = D_- = D = \mu k_B T$. The electrode potential is fixed to be $\phi = V$ at an inner fractal electrode and ϕ is fixed to be 0 at an outer circular surface at $r = L$, where r is a distance from the central point. In the thermal equilibrium state, the ion concentration satisfies

$$\nabla \rho_\pm \pm e/(k_B T) \rho_\pm \nabla \phi = 0. \tag{2}$$

By integrating Eq. (2), the thermal equilibrium distribution is obtained as

$$\rho_+(\mathbf{x}) = \rho_s \exp\{-e\phi(\mathbf{x})/k_B T\}, \quad \rho_-(\mathbf{x}) = \rho_s \exp\{e\phi(\mathbf{x})/k_B T\}, \tag{3}$$

where ρ_s is the concentration at $r = L$. By rescaling the space and time coordinates and the electric potential using the Debye length $\lambda_s = \{\epsilon k_B T_s/(e^2 \rho_s)\}^{1/2}$, $t_s = \epsilon/(\mu e^2 \rho_s)$, and $V_s = k_B T_s/e$ at a certain temperature T_s and a certain concentration ρ_s, Eq. (1) is rewritten as

$$\frac{\partial \rho_+}{\partial t} = T \nabla^2 \rho_+ + \nabla(\rho_+ \nabla \phi),$$

$$\frac{\partial \rho_-}{\partial t} = T \nabla^2 \rho_- - \nabla(\rho_- \nabla \phi),$$

$$\nabla^2 \phi = \rho_- - \rho_+, \tag{4}$$

where the variables and the control parameters are changed as $\rho_+/\rho_s \to \rho_+$, $\rho_-/\rho_s \to \rho_-$, $\mathbf{x}/\lambda_s \to \mathbf{x}$, $t/t_s \to t$, $Dt_s/\lambda_s^2 = T/T_s \to T$, and $\phi/V_s \to \phi$. The ion concentration is fixed to be ρ_0 and the electric potential ϕ is 0 at the outer boundary $r = L$. The dimensionless control parameters are the temperature T, the electrode potential V at the inner electrode, and the concentration ρ_0.

II. CAPACITANCE AND RESISTANCE OF ELECTRIC DOUBLE LAYER ON CIRCULAR ELECTRODE

First, we consider a simple case that the electrode is not fractal but a circle of radius R. The inner and outer electrodes

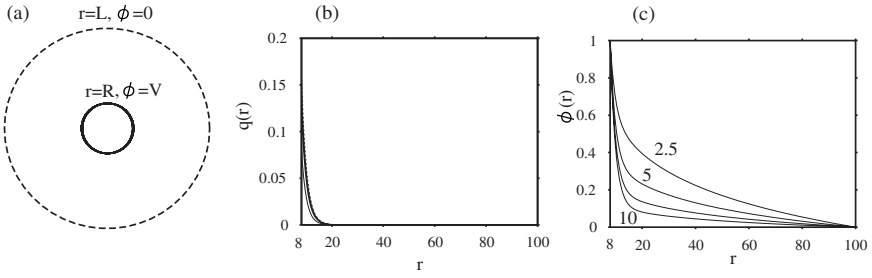

FIG. 1. (a) Circular electrodes with radius $r=R$ and $r=L$. Snapshot profiles of (b) $q(r)=\rho_- - \rho_+$ and (c) $\phi(r)$ at $t=2.5$, 5, 7.5, and 10 for $R=8$, $L=100$, $V=1$, $T=10$, and $\rho_0=1$.

are schematically shown in Fig. 1(a). We assume that V/T is smaller than 1 for the sake of simplicity because the strong nonlinear problem is more difficult. One-dimensional dynamics under the strong voltage was studied by Bazant *et al.* [10]. The circular symmetry is expected in this system, then, all variables depend only on r. The concentrations satisfy $\rho_+(r)=\rho_0 \exp[-\phi(r)/T]$, $\rho_-(r)=\rho_0 \exp[\phi(r)/T]$ in the equilibrium state. By using the approximation $\rho_+ \sim \rho_0(1-\phi/T)$ and $\rho_- \sim \rho_0(1+\phi/T)$ (which is satisfied for $|\phi|/T \ll 1$), the Poisson equation becomes

$$\frac{\partial^2 \phi}{\partial r^2} + \frac{1}{r}\frac{\partial \phi}{\partial r} - \frac{2\rho_0 \phi}{T} = 0. \tag{5}$$

The solution satisfying $\phi(R)=V$ and $\lim_{r\to\infty}\phi(r)=0$ is expressed as

$$\phi(r) = V I_0(r/\lambda)/I_0(R/\lambda),$$

where $I_0(r)$ is the modified Bessel function, $\lambda=\sqrt{T/(2\rho_0)}$ is the Debye length in our unit, and L is assumed to be sufficiently larger than $R+\lambda$. The Debye length represents the scale of the width of the electric double layer. The total charge Q stored in the electric double layer is expressed as

$$Q = \int_R^\infty dr(2\pi r)(\rho_- - \rho_+) = V\int_R^\infty dr(2\pi r) \times (2\rho_0/T) I_0(r/\lambda)/I_0(R/\lambda). \tag{6}$$

Because $\phi(r)$ decays from V to 0 in a length scale of the order λ, the integral is approximated as

$$Q \sim V\sqrt{2\rho_0/T}(2\pi R)(\alpha/2),$$

where α is a numerical factor of $O(1)$. The capacitance C is evaluated as

$$C \sim \sqrt{2\rho_0/T}(2\pi R)(\alpha/2). \tag{7}$$

The capacitance C has a form of $C=S/d$, where $S=2\pi R$ is the surface length of the condenser, and d is the width of the condenser, which is expressed as $d=2\lambda/\alpha$.

The Nernst-Planck equation is rewritten in a system with circular symmetry as

$$\frac{\partial \rho_+}{\partial t} = T\frac{1}{r}\frac{\partial}{\partial r}\left(r\frac{\partial \rho_+}{\partial r}\right) + \frac{1}{r}\frac{\partial}{\partial r}\left(r\rho_+ \frac{\partial \phi}{\partial r}\right),$$

$$\frac{\partial \rho_-}{\partial t} = T\frac{1}{r}\frac{\partial}{\partial r}\left(r\frac{\partial \rho_-}{\partial r}\right) - \frac{1}{r}\frac{\partial}{\partial r}\left(r\rho_- \frac{\partial \phi}{\partial r}\right). \tag{8}$$

We have performed a numerical simulation for $R=8$, $L=100$, $V=1$, $T=10$, and $\rho_0=1$. The initial condition is $\rho_+(r)=\rho_-(r)=\rho_0=1$. Figures 1(b) and 1(c) display snapshot profiles of $q(r)=\rho_-(r)-\rho_+(r)$ and $\phi(r)$ at $t=2.5$, 5, 7.5, and 10. The electric charge is only stored for $R<r<20$ as shown in Fig. 1(b). The profile of the potential $\phi(r)$ changes largely around $r=16$. When t is sufficiently large, $\phi(r)$ becomes zero around $r=20$. From these numerical results, it is seen that the electric potential $\phi(r)$ satisfies the Laplace equation

$$\frac{\partial^2 \phi}{\partial r^2} + \frac{1}{r}\frac{\partial \phi}{\partial r} = 0,$$

for $r>R_2=R+\alpha_2\lambda$, because there is no charge for $r>R_2$. Here, the width of the charged area is of the order of the Debye length and is expressed as $\alpha_2\lambda$ using another numerical factor α_2. The solution of the Laplace equation satisfying the boundary condition $\phi(L)=0$ is $\phi(r)=-\phi_2 \ln(r/L)$, where ϕ_2 is an integral constant. If the electric charge $Q(t)$ is stored inside of $r=R_2$ at a certain time t, the potential $\phi(r)$ at $r=R_2$ is estimated as $\phi(R_2)=V-Q(t)/C$. The integral constant ϕ_2 is therefore given by $\phi_2=[V-Q(t)/C]/\ln(L/R_2)$. Because the potential gradient is expressed as $\partial\phi/\partial r=-\phi_2/L$ at the outer circular boundary $r=L$, the time evolution of $Q(t)$ is evaluated as

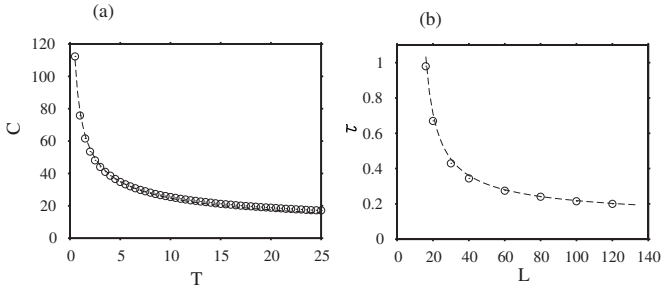

FIG. 2. (a) Numerically obtained capacitance C vs T for $R=8$, $L=40$, and $\rho_0=1$. The dashed curve is $C=\sqrt{2/T}\pi R\alpha$ with $\alpha=2.2$. (b) Numerically obtained relaxation rate $1/\tau$ as a function of L for $R=8$, $T=10$, and $\rho_0=1$. The dashed curve is $\alpha=1/\tau=\sqrt{8T}/[R\alpha \ln\{L/(R+\alpha_2\sqrt{2/T})\}]$ with $\alpha=2.2$ and $\alpha_2=0.8$.

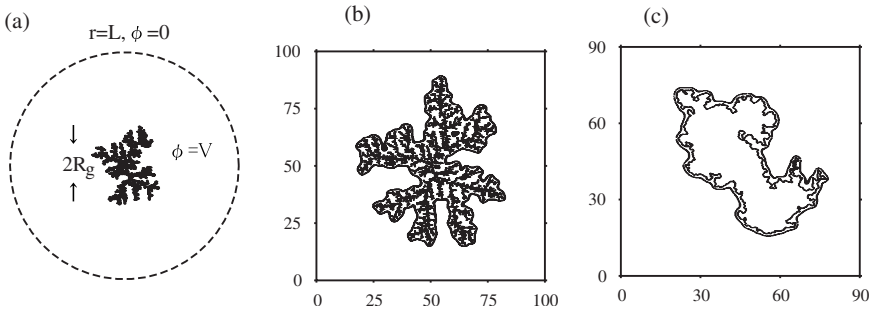

FIG. 3. (a) Inner fractal electrode of radius R_g of gyration and the outer electrode at $r=L$. (b) A DLA cluster and a contour curve of $\phi=0.5$ around the DLA electrode. (c) Outermost surface of a critical percolation cluster and a contour curve of $\phi=0.5$ around the fractal electrode for $T=5$, $\rho_0=1$, $L=50$, and $V=1$.

$$\frac{dQ}{dt} = 2 \times 2\pi L \times \rho_0 \times \phi_2/L = \frac{4\pi\rho_0[V - Q(t)/C]}{\ln(L/R_2)}, \quad (9)$$

from the surface integral of the current $J=\rho_0 \partial\phi/\partial r$ at the outer circular boundary. Here, we have used an assumption that the diffusion current by $\partial\rho_+(r)/\partial r$ and $\partial\rho_-/\partial r$ is zero at $r=L$, which has been numerically confirmed, and it is seen also from $\partial q(r)/\partial r=0$ at $r=L$ in Fig. 1(b). The relaxation time for the charging process is therefore given by

$$\tau = C \ln(L/R_2)/(4\pi\rho_0), \quad (10)$$

and the resistance is evaluated as $R=\ln(L/R_2)/(4\pi\rho_0)$ by the relation $\tau=RC$.

Figure 2(a) displays numerically obtained capacitance as a function of T for $R=8$, $L=40$, and $\rho_0=1$. The dashed curve is $C=\sqrt{2/T}\pi R\alpha$ with $\alpha=2.2$. Figure 2(b) displays numerically obtained decay rates $1/\tau$ as a function of L for $R=8$, $T=10$, and $\rho_0=1$. The dashed curve is $1/\tau = \sqrt{8T}/[R\alpha \ln\{L/(R+\alpha_2\sqrt{2/T})\}]$ with $\alpha=2.2$ and $\alpha_2=0.8$. Good agreement is seen between numerical results and theoretical curves.

III. CAPACITANCE OF ELECTRIC DOUBLE LAYERS ON FRACTAL ELECTRODES

In this section, we study the capacitance stored in the electric double layers around fractal electrodes. Only the inner electrode is fractal and the outer electrode is circular as shown schematically in Fig. 3(a). In this paper, we use DLA clusters and critical percolation clusters as fractal electrodes because the geometrical properties are well-understood. The electric double layer is formed around the electrode surface. Only the charge stored around the outermost surface is effective for the capacitance because the electric charge cannot penetrate into the inner space of the electrode, even if there is vacant space in the inner space. For a DLA cluster, every site belongs to the outermost surface. The fractal dimension of the outermost surface is therefore equal to $D_f=1.71$. If the raidus of gyration is expressed as R_g, the total surface site number is scaled as $N_s \sim R_g^{D_f}$. For a critical percolation cluster, the fractal dimension of the outermost surface is evaluated as nearly $4/3 \sim 1.3$, which is different from the fractal dimension 1.895 of the whole critical percolation cluster [11].

The DLA cluster and the critical percolation cluster are constructed on a square lattice of grid size $\Delta x=0.2$. We have performed direct numerical simulations of the Nernst-Planck-Poisson equation (4) with a simple Euler method of grid size $\Delta x=0.2$ and time step $\Delta t=0.001$. The electric potential ϕ is fixed to be V on the fractal sets. We have imposed no flux boundary condition on the fractal surfaces. That is, the currents $J=T\nabla\rho_\pm \pm \rho_\pm \nabla\phi$ are zero at the fractal surface. The outer boundary is set on a circle of radius $r=L$, where ϕ is fixed to be 0 and the concentrations are $\rho_\pm=\rho_0$. The radius r is measured as a distance from the seed for the DLA cluster or from the center of mass for the critical percolation cluster. We can roughly estimate the capacitance of the electric double layers on fractal electrodes. The electric charge is stored in the area of the width of the order of the Debye length around the fractal electrode. Figures 3(b) and 3(c) display fractal electrodes and contour curves of $\phi=V/2=0.5$ around the fractal electrodes at $L=50$, $T=5$, $\rho_0=1$, and $V=1$ in the equilibrium state, which was obtained by direct numerical simulations. A DLA cluster and a critical percolation cluster are used as the fractal electrodes, respectively, in Figs. 3(b) and 3(c). The fine structure of the fractal surface becomes unclear because of the finite scale of the Debye length. Similarly to the box counting method to calculate the fractal dimension, the number N_λ of the surface elements measured by the unit of the Debye length is evaluated as $N_\lambda \sim N_s(\Delta x/\lambda)^{D_f}$, where N_s is the total number of the surface sites counted by the smallest length scale Δx in our numerical simulation. The effective surface length is therefore $S_{eff}=N_\lambda\lambda=N_s\Delta x^{D_f}/\lambda^{D_f-1}$. The width of the electric double layer is evaluated as $2\lambda/\alpha$. The capacitance is therefore estimated as

$$C \sim \frac{S_{eff}\alpha}{2\lambda} \sim R_g^{D_f}\left(\frac{2\rho_0}{T}\right)^{D_f/2}. \quad (11)$$

Figure 4 displays numerical results of the capacitance of the electric double layer around DLA clusters. Figure 4(a) displays a relation of C vs R_g for several sizes of DLA clusters for $T=5$, $V=1$, $L=50$, and $\rho_0=1$. The dashed line denotes $C \sim R_g^{1.7}$. Figure 4(b) displays a relation of C vs T, and the dashed line denotes $C \sim 1/T^{0.83}$ for $N_s=8765$, $V=1$, $L=50$, and $\rho_0=1$. Figure 4(c) displays a relation of C vs ρ_0 for $N_s=8765$, $V=1$, $L=50$, and $T=4$, and the dashed line is $\rho_0^{0.83}$.

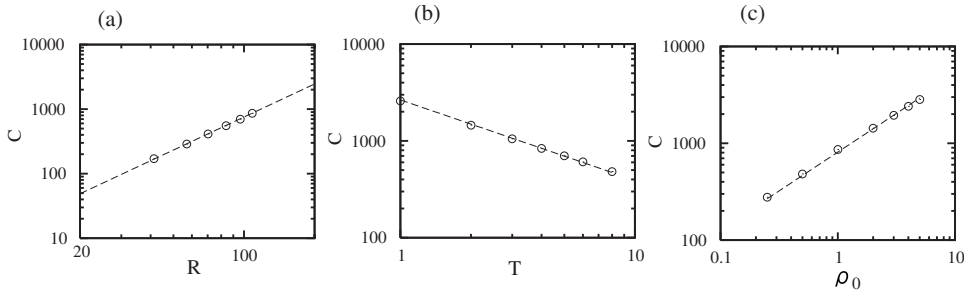

FIG. 4. (a) Numerically obtained capacitance C vs radius R_g of gyration for several sizes of DLA clusters for $T=5$, $V=1$, $L=50$, and $\rho_0=1$. The dashed line denotes $C=R_g^{1.7}$. (b) C vs T at $V=1$, $N_s=8765$, $L=50$, and $\rho_0=1$, and the dashed line denotes $C\sim 1/T^{0.83}$. (c) C vs ρ_0 at $L=50$, $V=1$, $N_s=8765$, and $T=4$, and the dashed line denotes $\rho_0^{0.83}$.

The numerically obtained exponent 0.83 is close to $D_f/2=0.85$. Figure 5 displays the capacitance for the critical percolation clusters. Figure 5(a) displays C as a function of R_g (R_g was calculated for the outermost surface) at $T=5$, $V=1$, $L=50$, and $\rho_0=1$. The dashed line is $C\sim R_g^{1.3}$. Figure 5(b) displays a relation of C vs T for $\rho_0=1$, $V=1$, $L=50$, and $N_s=1972$. The dashed line denotes $C\sim 1/T^{0.665}$. Figure 5(c) displays a relation of C vs ρ_0 at $N_s=1972<V=1$, $L=50$, and $T=3$. The dashed line is $C\sim\rho_0^{1.3}$. These numerical results are consistent with the theoretical estimate (11). We have also numerically confirmed that the capacitance does not depend on the size L of the outer circular electrode.

IV. CHARGING DYNAMICS IN ELECTRIC DOUBLE LAYERS AROUND FRACTAL ELECTRODES

In this section, we consider time evolution of the charging process around the fractal electrodes. The electric potential at the fractal electrode is suddenly changed from 0 to V, and the charging process in the electric double layer is investigated. This is interpreted as a problem to study the dynamical response of the system for the stepwise force. The topic of dynamical response of fractal electrodes has been intensively studied in the context of constant-phase angle (CPA) impedance for the ac voltage, which was already observed in the 1920s. The CPA impedance has a form of $Z(\omega)=R+k(i\omega)^{-p}$. Levie proposed a transmission line model with $p=1/2$ for porous electrodes [12]. Sapoval, Pajkossy-Nyikos, and Leibig-Halsey studied the CPA impedance for fractal electrodes and showed the exponent p is related to the fractal dimension D_f [13–16]. The CPA impedance was also studied experimentally by Larsen *et al.* and Pajkossy-Kyikos [17,18]. The impedance $Z(\omega)$ is related to the relaxation function of the current $I(t)=dQ(t)/dt$ for the stepwise electrode potential $\phi=V\theta(t)$ [$\theta(t)$ is the Heaviside step function] as $I(\omega)=V/\{i\omega Z(\omega)\}$, where $I(\omega)=\int_0^\infty I(t)e^{-i\omega t}dt$, if the linear response relation is assumed. For example, the normal exponential relaxation in the RC circuit is directly related to the normal behavior of the impedance $Z(\omega)=R+1/(i\omega C)$ with $p=1$. The CPA behavior with $p<1$ is usually considered to be related to the power law relaxation of $I(t)$. Halsey and Leibig suggested a stretched exponential relaxation of the form $I(t)\sim\exp(-\alpha t^\beta)$ for the self-similar electrodes. They proposed a relation between the multifractal exponent $\tau(2)$, the surface dimension D_s, and the exponent β as $\beta=\tau(2)/D_s$ [19]. For the DLA electrode, the exponent β is estimated as $\beta=0.52$. This type of stretched exponential relaxation is experimentally observed in various materials such as glasses and amorphous. Kohrausch first studied this type of relaxation, and Williams-Watts studied it further, and the stretched exponential relaxation is often called a Kohrausch-Williams-Watts (KWW) type relaxation [20]. The anomalous relaxation including the KWW relaxation and the power law relaxation and the anomalous diffusion are studied in [21,22]. Although many authors studied the dynamic response of the systems with fractal surfaces, the dynamics of ions and the finite size effect of the Debye length were not explicitly involved in the previous theories. On the other hand, the charging process of the ions into the area of the order of the Debye length around the fractal electrode is essential in the Nernst-Planck-Poisson equation, and a new

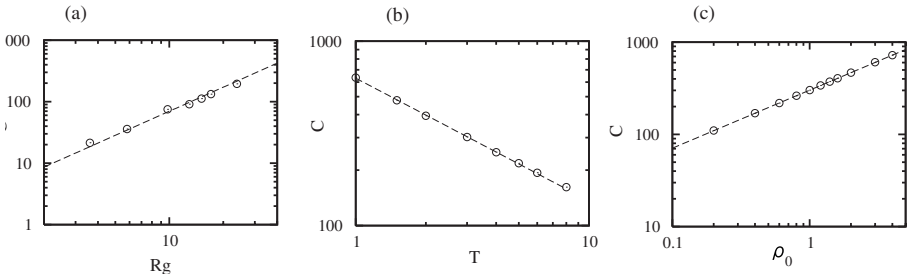

FIG. 5. (a) Numerically obtained C vs R_g in the outermost surface for several sizes of critical percolation clusters for $T=5$, $V=1$, $L=50$, and $\rho_0=1$. The dashed line denotes $C\sim R_g^{1.3}$. (b) C vs T for $\rho_0=1$, $V=1$, $L=50$, and $N_s=1972$. The dashed line is $C\sim 1/T^{0.665}$. (c) C vs ρ_0 for $N_s=1972$, $V=1$, $L=50$, and $T=3$. The dashed line is $C\sim\rho_0^{1.3}$.

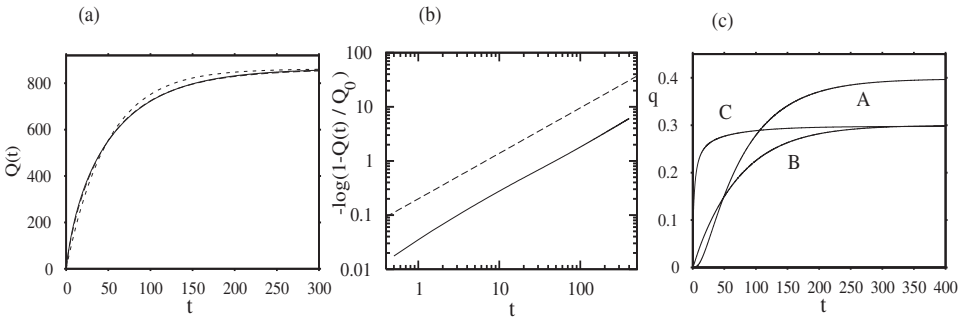

FIG. 6. (a) Time evolution of the total charge $Q(t)$ for a DLA electrode for $T=5$, $N_s=10\,759$, $L=50$, and $\rho_0=1$. The solid curve denotes the numerical result, the almost overlapped dashed curve is $Q=Q_0\{1-\exp[-(t/\tau)^\beta]\}$ with $\beta=0.84$, and the dotted curve is $Q=Q_0[1-\exp(-t/\tau)]$. (b) Double-logarithmic plot of $-\ln[1-Q(t)/Q_0]$ as a function of t. The dashed line is a stretched exponential curve with $\beta=0.84$. (c) Three time evolutions of $q(x,y)=\rho_-(x,y)-\rho_+(x,y)$ at different points A, B, and C, respectively, at $(x,y)=(49.4,49.4)$, (47.2, 64.4), and (54, 89).

aspect of the charging dynamics might be found in the direct numerical simulation of our model.

In our simulations, $\rho_+=\rho_-=\rho_0$ and the electrode potential ϕ is set to $V=1$ at $t=0$. Then, the time evolution of the total charge $Q(t)$ stored in the electric double layer is measured. This type of simulation is relevant to the realistic charging process of the electric double-layer capacitors. From the result in Sec. II, the relaxation time τ is expected to be $\tau=C\ln(L/R_2)/(4\pi\rho_0)$, where C is the capacitance for the fractal electrode studied in the previous section and R_2 is a characteristic radius of the fractal surface. The relaxation time is therefore estimated as

$$\tau \sim R_g^{D_f}\left(\frac{2\rho_0}{T}\right)^{D_f/2}\frac{\ln(L/R_2)}{4\pi\rho_0} \propto T^{-D_f/2}\rho_0^{D_f/2-1}\ln(L/R_2). \tag{12}$$

However, the distance between the fractal surface and the outer boundary at $r=L$ is randomly distributed in case of fractal electrodes. Besides, the charging process might be delayed deep in fiord regions in the fractal surface because it seems to take a long time for ions to approach such intricate regions. The inhomogeneities of the local electric field around the fractal surface were taken into consideration also in previous studies [15,16]. That is, the local electric field is much larger at a protrusion than in a protected region and the relaxation time is expected to be small at the protrusion. It is therefore expected that the relaxation time is locally distributed and the charging process might not obey a simple exponential law as in the case of the circular electrode. The power law relaxation and the stretched exponential relaxation are often interpreted as the broad distribution of the relaxation time.

Figure 6(a) displays a time evolution of the total charge $Q(t)$ for a DLA cluster at $T=5$, $N_s=10\,759$, $L=50$, and $\rho_0=1$. The solid curve denotes the numerical result, the dashed curve is $Q=Q_0[1-\exp\{-(t/\tau)^\beta\}]$ with $Q_0=861.8$, $\tau=48.6$, and $\beta=0.84$. (The dashed curve is overlapped with the solid curve and the difference is almost invisible.) The dotted curve is $Q=Q_0[1-\exp(-t/\tau)]$ with $Q_0=861.8$ and $\tau=48.6$. The relaxation time τ was evaluated as a time when $Q(t)$ satisfies $Q(t)/Q_0=1-1/e$. The stretched exponential law is better than a simple exponential law. Figure 6(b) displays a double-logarithmic plot of $-\ln[1-Q[t)/Q_0]$ vs t. The linear curve in this plot implies that the time evolution obeys a stretched exponential law and the slope of the linear line represents the exponent β. The dashed line is a stretched exponential curve with $\beta=0.84$. Figure 6(c) displays three time evolutions of $q(x,y,t)=\rho_-(x,y,t)-\rho_+(x,y,t)$ at three different points A, B, and C, respectively at $(x,y)=(49.4,49.4)$, (47.2, 64.4), and (54, 89), which are in contact with the fractal electrode by the smallest size scale Δx. The distances between the seed of the DLA cluster located at (50,50) and the three points are, respectively, small, intermediate, and large. The time evolution at point A near the center is very slow. The time evolution and the relaxation time are rather different for the three points. We have calculated the average $\langle\tau_l\rangle$ and the variance of the local relaxation time τ_l for all points satisfying $q(x,y)>0.01$ in the equilibrium state. Figure 7(a) shows the sites satisfying $\tau_l<\langle\tau_l\rangle$ among the sites in contact with the fractal electrodes. The local relaxation time τ_l is small in the outer region. It is probably because the distance from the outer boundary is small in the region. In our model, we can explicitly calculate the distribution of the local relaxation time by evaluating the relaxation time at each point. Figure 7(b) displays a histogram of the local relaxation time. The distribution of the local relaxation time is rather wide, and it is a possible origin of the

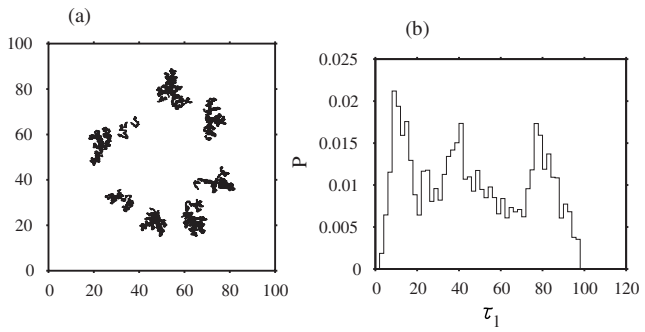

FIG. 7. (a) The sites satisfying $\tau_l<\langle\tau_l\rangle$ among the sites in contact with the fractal electrodes. (b) Histogram of the local relaxation time for the sites satisfying $q(x,y)>0.01$.

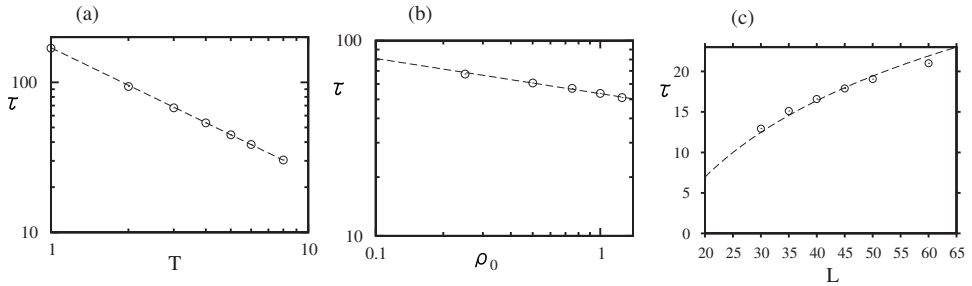

FIG. 8. (a) Relaxation time τ vs T at $L=100$, $N_s=8765$, $V=1$, and $\rho_0=1$, and the dashed line is $\tau\sim 1/T^{0.83}$. (b) τ vs ρ_0 at $L=100$, $N_s=8765$, $V=1$, and $T=4$, and the dashed line is $\tau\sim 1/\rho_0^{0.18}$. (c) τ vs L for $T=5$, $V=1$, $N_s=2099$, and $\rho_0=1$, and the dashed curve is $C/(4\pi)\ln(L/R_2)$.

stretched exponential law of $Q(t)$ because the total charge is the sum of the local charge as $Q(t)=\int\int dxdyq(x,y,t)$. However, the distribution of the local relaxation time does not seem to obey a simple function, so we do not understand the relation of the stretched exponential law of $\beta=0.84$ and the histogram of τ_l well. The numerically obtained value β is different from $\beta=0.52$ predicted by Halsey and Leibig, thus the relation with their theory is not well-understood.

We have calculated the relaxation time τ of $Q(t)$ by changing several control parameters. Figure 8(a) shows τ as a function of T, and the dashed line is $\tau\sim 1/T^{0.83}$ at $L=100$, $N_s=8765$, $V=1$, and $\rho_0=1$. Figure 8(b) shows a relation of τ vs ρ_0 at $L=100$, $N_s=8765$, $V=1$, and $T=4$, and the dashed line is $\tau\sim 1/\rho_0^{0.18}$. The exponent 0.18 is close to $1-D_f/2=0.15$, but it is slightly larger than the theoretical value. Figure 8(c) shows τ as a function of L at $T=5$, $V=1$, $N_s=2099$, and $\rho_0=1$, and the dashed curve is $C/(4\pi)\ln(L/R_2)$, where $C=171.0$ and the characteristic radius $R_2=12.0$ is approximated as $1.46R_g$ or $R_g+2.4\sqrt{T/2}$. These numerical results are consistent with the theoretical estimate (12), although the time evolution does not obey a simple exponential law. The exponent β of the stretched exponential law does not depend on T or ρ_0 strongly. However, the exponent β depends on the cluster size of the electrodes. For example, β decreases as $\beta=0.96$, 0.93, 0.91, 0.88, 0.88, 0.85, and 0.83 when the radius of gyration is increased as $R_g=8.26$, 11.4, 14.1, 16.8, 19.3, and 21.7 at $L=50$, $V=1$, $T=5$, and $\rho_0=1$. For small R_g, the fractal electrode can be approximated as a circular electrode, which might be a reason that the exponent β is close to 1.

We have performed the same type of analyses for the critical percolation clusters and obtained similar results. Figure 9(a) displays a time evolution of $Q(t)$ for $L=45$, $T=5$, $N_s=1978$, and $\rho_0=1$. The solid curve is a numerical result and the overlapped dashed curve is $Q=Q_0\{1-\exp[-(t/\tau)^\beta]\}$ with $Q_0=216.7$, $\tau=10.55$, and $\beta=0.72$, and the dotted curve is an exponential curve $Q=Q_0[1-\exp(-t/\tau)]$. It implies that the charging dynamics obeys a stretched exponential law. Figure 9(b) displays three time evolutions of $q(x,y,t)$ for three different points A, B, and C located at (44.4, 55.6), (45, 30), and (77.4, 38). The relaxation time is rather large for point A at (44.4, 55.6), which is located in a deep fiord as shown in Fig. 9(c). We have calculated the local relaxation time τ_l at all sites satisfying $q(x,y)>0.01$ in the equilibrium state also for this fractal electrode. The local relaxation time is widely distributed between $1.96<\tau_l<48.5$. It is a possible reason for the stretched exponential relaxation. The average value of the relaxation time is calculated as 12.9, and the standard deviation is 10.4. All the sites in contact with the fractal electrode are plotted with dots in Fig. 9(c) and the sites satisfying $\tau_l<\langle\tau_l\rangle$ are shown by thick marks in Fig. 9(c). It is seen in Fig. 9(c) that the local relaxation time is relatively large in the concave bay area.

Figure 10(a) displays the relaxation time τ of $Q(t)$ as a function of T at $L=50$, $V=1$, $\rho=1$, and $N_s=1978$, and the dashed curved is $\tau\sim 1/T^{0.68}$. Figure 10(b) displays a relation

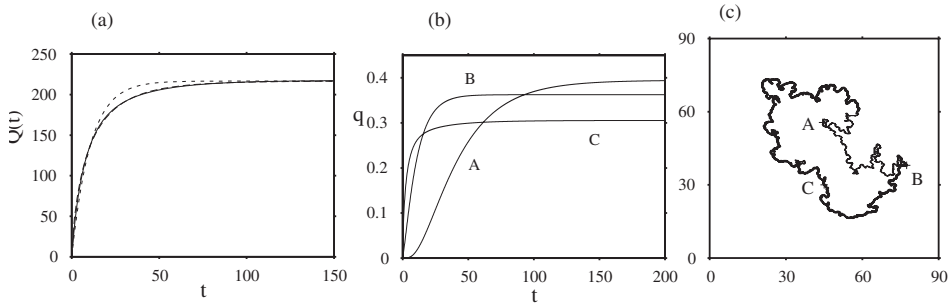

FIG. 9. (a) Time evolution of $Q(t)$ at $L=45$, $T=5$, $N_s=1978$, and $\rho_0=1$. The solid curve is numerical results and the overlapped dashed curve is $Q=Q_0\{1-\exp[-(t/\tau)^\beta]\}$ with $\beta=0.72$, and the dotted curve is a exponential curve $Q=Q_0[1-\exp(-t/\tau)]$. (b) Three time evolutions of $q(x,y,t)=\rho_-(x,y,t)-\rho_+(x,y,t)$ at different points A, B, and C located at (44.4, 55.6), (45, 30), and (77.4, 38). (c) The sites in contact with the fractal electrode are plotted with dots. The local relaxation time τ_l is smaller than $\langle\tau_l\rangle$ in the region marked by thick dots. The three points A, B, and C are denoted by the letters.

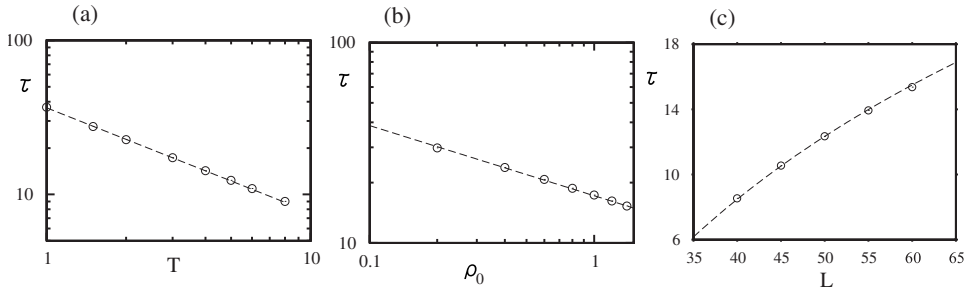

FIG. 10. (a) Relaxation time τ of $Q(t)$ vs T at $L=50$, $V=1$, $\rho=1$, and $N_s=1978$, and the dashed curved is $\tau \sim 1/T^{0.68}$. (b) τ vs ρ_0 at $L=50$, $V=1$, $T=3$, and $N_s=1978$, and the dashed curve is $\tau \sim 1/\rho_0^{0.35}$. (c) τ vs L at $L=50$, $V=1$, $N_s=1978$, $\rho_0=1$, and $T=5$, and the dashed curved is $C/(4\pi)\ln(L/R_2)$.

of τ vs ρ_0 at $L=50$, $V=1$, $T=3$, and $N_s=1978$, and the dashed curve is $\tau \sim 1/\rho_0^{0.35}$. The exponent 0.35 is close to $1-D_f/2=0.33$. Figure 10(c) displays τ as a function of L at $V=1$, $N_s=1978$, $\rho_0=1$, and $T=5$, and the dashed curved is $C/(4\pi)\ln(L/R_2)$ where $C=216.68$ and $R_2=24.5 \sim R_g+1.15\{T/(2\rho_0)\}^{1/2}$. These results are consistent with the theoretical estimate (12). The exponent β of the stretched exponential law depends also on the system size L. The exponent β increases as $\beta=0.65$, 0.72, 0.75, 0.76, and 0.78, when L is increased as $L=40$, 45, 50, 55, and 60 at $V=1$, $T=5$, $N_s=1978$, and $\rho_0=1$.

V. SUMMARY AND DISCUSSION

We have proposed a simple model based on the Nernst-Planck-Poisson equation for the electric double layer around fractal electrodes and performed direct numerical simulations of the model. As random fractal electrodes, we have used DLA clusters and critical percolation clusters because the fractal dimensions are well-known.

We have roughly estimated the capacitance and the relaxation time of the electric double layer on fractal electrodes. The capacitance and the relaxation time depend on the temperature and the concentration by power laws, and the exponents depend on the fractal dimension of the electrodes. We have confirmed the scaling relation with direct numerical simulations. We have further found a stretched exponential law in the time evolution of $Q(t)$. In our model, the local relaxation time can be measured at each point in the electric double layer. The stretched exponential law seems to be due to the wide distribution of the local relaxation time, however, the details are not well-understood.

We have performed numerical simulations in a finite system such as $R_g \sim 10$ and $L \sim 50$, which correspond to the order of several hundred angstroms because the Debye length is the order of tens of angstroms. However, the scaling law of the capacitance is expected to be applied to the usual macroscopic experimental situation because the capacitance does not depend on the size L of the outer electrode and depends on R_g via a power law. However, the exponent of β depends on R_g and L. We are not sure now that the stretched exponential law is satisfied in a macroscopic system.

In this paper, we have assumed that the electrode potential V is not so strong. In this case, the stored total charge Q_0 is proportional to the electrode potential V. In the case of stronger electrode potential, Q_0 might depend nonlinearly on V. We have also assumed simple fractals for the electrodes, which cannot be interpreted as porous electrodes. As Leibig and Halsey suggested in [16], the CPA behavior characterized by the power law is expected to appear in porous media. We will investigate the charging dynamics in such porous media in the next step, using the Nernst-Planck-Poisson equation. We have further neglected the Helmholtz layer for the electric double layer and various size effects of ions and water molecules. Our model is therefore too simple to compare realistic experiments now. We would like to generalize our model system and study the charging dynamics of the electric double layer in more realistic systems in the future.

[1] S. Sarangapani, B. V. Tilak, and C. P. Chen, J. Electrochem. Soc. **143**, 3791 (1996).
[2] B. E. Conway, V. Birss, and J. Wojtowicz, J. Power Sources **66**, 1 (1997).
[3] W. G. Rothschild, *Fractals in Chemistry* (Wiley, New York, 1998).
[4] J. Ross Macdonald and S. Kenkel, J. Chem. Phys. **80**, 2168 (1984).
[5] M. S. Kilic, M. Z. Bazant, and A. Ajdari, Phys. Rev. E **75**, 021501 (2007).
[6] T. Kaplan, L. J. Gray, and S. H. Liu, Phys. Rev. B **35**, 5379 (1987).
[7] H. Samavari, A. Hajimiri, A. R. Shahani, G. N. Nasserbakht, and T. H. Lee, IEEE J. Solid-State Circuits **33**, 2035 (1988).
[8] G. Gouy, J. Phys. (Paris) **9**, 457 (1910).
[9] D. L. Chapman, Philos. Mag. **25**, 475 (1913).
[10] M. Z. Bazant, K. Thornton, and A. Ajdari, Phys. Rev. E **70**, 021506 (2004).
[11] T. Grossman and A. Aharony, J. Phys. A **19**, L745 (1986).
[12] R. De Levie, Electrochim. Acta **9**, 1231 (1964).
[13] B. Sapoval, Solid State Ionics **23**, 253 (1987).
[14] L. Nyikos and T. Pajkossy, Electrochim. Acta **30**, 1533

(1985).
[15] T. C. Halsey, Phys. Rev. A **35**, 3512 (1987).
[16] M. Leibig and T. Halsey, Electrochim. Acta **38**, 1985 (1993).
[17] A. E. Larsen, D. G. Grier, and T. C. Halsey, Phys. Rev. E **52**, R2161 (1995).
[18] T. Pajkossy and L. Nyikos, Electrochim. Acta **34**, 171 (1989).
[19] T. C. Halsey and M. Leibig, Phys. Rev. A **43**, 7087 (1991).
[20] G. Williams and D. C. Watts, Trans. Faraday Soc. **66**, 80 (1970).
[21] J. Klafter and M. Shlesinger, Proc. Natl. Acad. Sci. U.S.A. **83**, 848 (1986).
[22] R. Metzler and J. Klafter, Phys. Rep. **339**, 1 (2000).